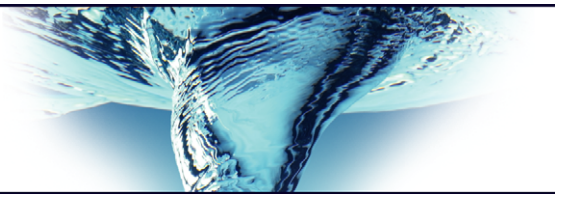
J. Fluid Mech. (2013), *vol.* 733, R5, doi:10.1017/jfm.2013.444



JFM RAPIDS
journals.cambridge.org/rapids

Unsteady pitching flat plates

Kenneth O. Granlund[1],†, Michael V. Ol[1] and Luis P. Bernal[2]

[1]Air Force Research Laboratory, Wright-Patterson AFB, OH 45433, USA
[2]Department of Aerospace Engineering, University of Michigan, Ann Arbor, MI 48109, USA

(Received 5 June 2013; revised 31 July 2013; accepted 19 August 2013)

Direct force measurements and qualitative flow visualization were used to compare flow field evolution versus lift and drag for a nominally two-dimensional rigid flat plate executing smoothed linear pitch ramp manoeuvres in a water tunnel. Non-dimensional pitch rate was varied from 0.01 to 0.5, incidence angle from 0 to 90°, and pitch pivot point from the leading to the trailing edge. For low pitch rates, the main unsteady effect is delay of stall beyond the steady incidence angle. Shifting the time base to account for different pivot points leads to collapse of both lift/drag history and flow field history. For higher rates, a leading edge vortex forms; its history also depends on pitch pivot point, but linear shift in time base is not successful in collapsing lift/drag history. Instead, a phenomenological algebraic relation, valid at the higher pitch rates, accounts for lift and drag for different rates and pivot points, through at least 45° incidence angle.

Key words: low-dimensional models, nonlinear dynamical systems, separated flows, vortex flows, wakes/jets

1. Introduction

The pitching flat plate in a steady free stream has long been a standard problem in unsteady aerodynamics, where one is interested in relating history of the aerodynamic force coefficients and flow field evolution to the motion history. Motivations range from manoeuvring aircraft (Harper & Flanigan 1950), to landing and 'perching' of birds (Carruthers, Thomas & Taylor 2007) or small manmade vehicles mimicking birds (Reich *et al.* 2011), to flapping wings of insects or insect-like manmade fliers (Chakravarthy, Grant & Lind 2012), to helicopter dynamic stall (McCroskey, Carr & McAlister 1976) and to classical aeroelasticity (Theodorsen 1935) and its modern generalizations (McGowan *et al.* 2011; Baik *et al.* 2012). Lift and drag coefficients depart from classical attached-flow relations as the plate encounters flow separation, with strong dependency on pitch rate and chordwise location of pivot point. We report

† Email address for correspondence: kenneth.granlund@wpafb.af.mil

© Cambridge University Press 2013. This is a work of the U.S. Government and is not subject to copyright protection in the United States.

https://doi.org/10.1017/jfm.2013.444 Published online by Cambridge University Press

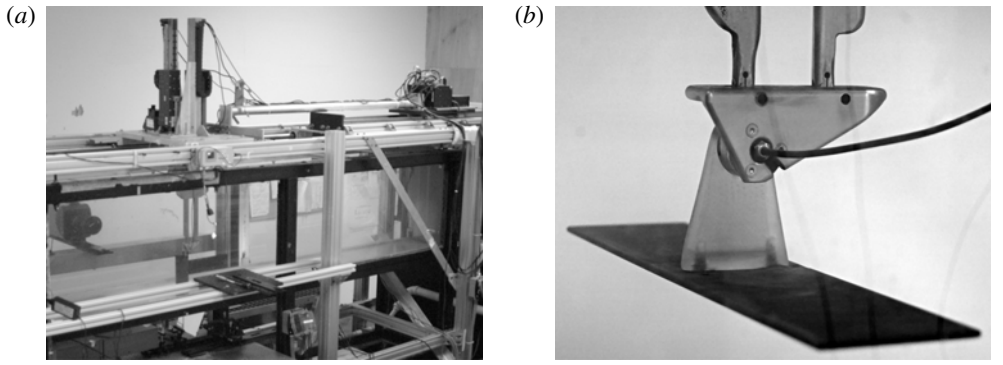


FIGURE 1. Water tunnel with motion mechanism (*a*) and flat plate model (*b*).

a broad experimental parametric study of these kinematic variables for a nominally two-dimensional rigid thin flat plate, generalizing scaling of lift and drag with non-dimensional pitch rate proposed by Strickland & Graham (1987) to account for pivot point, and relate such scaling to the formation, growth and pinch-off of leading edge vortices (LEVs) (Ringuette, Milano & Gharib 2007). The present experiments are at $Re = 20k$, angle of incidence $\theta = 0$–$90°$, and reduced pitch rate range from $K = 0.01$ through 0.5 ($K = \dot{\theta}c/2U_\infty$).

2. Experimental set-up

Measurements were taken in the US Air Force Research Laboratory's Horizontal Free-surface Water Tunnel (figure 1*a*) (Ol *et al.* 2009). The tunnel has a 4:1 contraction and 0.46 m wide by 0.61 m high test section, and is fitted with a three degree of freedom electric motion rig. Two linear motors drive the test article vertically, with a third linear motor operating horizontally, resulting in independent control of pitch or rotation about some specified pivot point. Tunnel free stream speed range is 0.03–0.45 m s^{-1}. The test article in figure 1(*b*) is a carbon-fibre flat plate with 0.02 thickness to chord ratio, round leading and trailing edges, 76.2 mm chord and 1 mm tip-to-sidewall gap, for physical aspect ratio of 6. Reynolds number is 20 000 based on chord and free stream speed.

Force data are taken with an ATI Nano25 IP68 6-component load cell connected to the plate's centreplane via a 0.5c-tall strut. The apparent mass of the water accelerated along with the model is equivalent to a circular cylindrical slug of fluid with length the same as that of the model, and diameter equal to the plate chord. This is $\approx$10 times the mass of the model, sting, and metric portion of the balance, thus obviating dynamic tares for testing in air (Barlow *et al.* 1999). The manufacturer's quoted uncertainty bounds for the Nano25 load cell are $\leqslant 0.28N$; this is commensurate with the highest 95 % confidence interval in dimensional normal force in figure 2(*b*).

A static tare sweep over $0° < \theta < 90°$ is performed with 500 samples of data every 2°. Because the pitch angle is known throughout the motion, and the position error is $<0.02°$ (Ol *et al.* 2009), the static axial force, normal force and pitching moment due to static model/sting/mount weight can be subtracted from the unsteady force data. Unsteady data is recorded at 1 kHz and low-pass filtered in hardware at $f = 35$ Hz (0.1 convective time). Then a moving average of 11 points is taken, followed by fourth-order Chebychev II low-pass filter with -20 dB attenuation of the stopband to

https://doi.org/10.1017/jfm.2013.444 Published online by Cambridge University Press

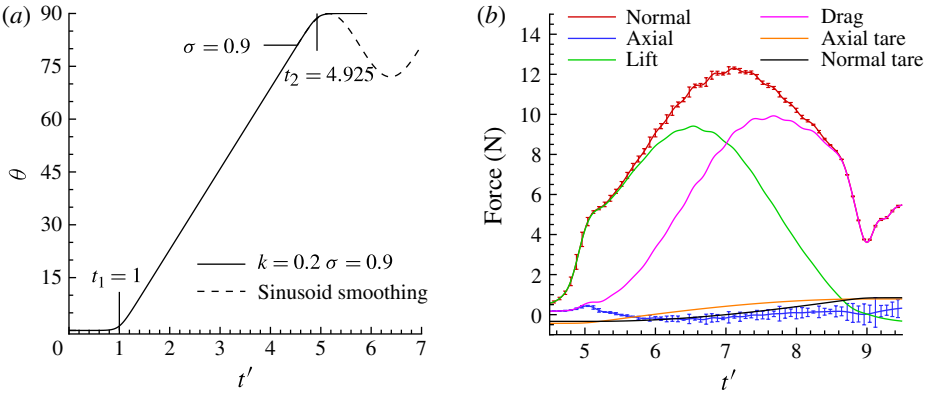


FIGURE 2. Angle of attack versus convective time for $K = 0.2$, $\theta_{max} = 90°$, $\sigma = 0.9$ and the corresponding sinusoid ramp corner smoothing (a) and breakdown of forces and uncertainties for $K = 0.2$, $x_p/c = 0$ motion (b).

preserve fast non-circulatory load spikes. The cutoff frequency is five times the motion frequency, assuming the ramp motion being a 1/4-wave. To preclude the time shift of data in the passband, the forward–backward filtering technique with the MATLAB filtfilt command is used.

The flow field is visualized by planar laser fluorescence. A high concentration of Rhodamine 6G in water is injected at the leading and trailing edges at 5/8, 6/8 and 7/8 span locations by a positive-displacement pump with a prescribed volumetric infusion rate, via 0.5 mm internal-diameter rigid lines glued to the surface of the plate, as documented by Ol *et al.* (2009). The dye is illuminated by an Nd:YLF 527 nm pulsed laser sheet of 1.5 mm thickness at 50 Hz and images are recorded with a PCO DiMax high-speed camera through a Nikon PC-E 45 mm Micro lens. An orange Wratten #21 filter removes the incident and reflected laser light since the dye fluorescence wavelength is 566 nm.

The pitch motion is nominally constant rate, or zero acceleration. But for this to be literally true, pitch acceleration would be infinite at $\theta = 0$ and 90°. Parameter studies on smoothing transients for pitch-ramp motions have been considered before (Koochesfahani & Smiljanovski 1993). Smoothing transients not only make a given nominally constant-rate motion realizable in an experiment, but are also important from the viewpoint of non-circulatory or acceleration-dependent aerodynamic forces. The upper limit for maximum attainable reduced pitch rate, for a given Reynolds number, is excitation of the model/sting/balance natural frequency, which confounds measurement of non-circulatory aerodynamic forces with oscillations in the apparent aerodynamic force coefficients due to structural vibrations. To obtain C^∞ smoothing, a modification of the hyperbolic-cosine function suggested by Eldredge, Toomey & Medina (2010) is fitted to the pitch ramp motion and shown in figure 2. The constants t'_1 and t'_2 determine the sharp ramp corner start and end. Here σ controls the amplitude of smoothing, in the sense of $(1 - \sigma)$ being the amplitude of the sine-wave tangent to the linear ramp and approximately equal to the size of the 'smoothing corner'.

$$\theta = \frac{K}{a} \ln \left[\frac{\cosh\left(a\left(t' - t'_1\right)\right)}{\cosh\left(a\left(t' - t'_2\right)\right)} \right] + \frac{\theta_{max}}{2} \tag{2.1}$$

https://doi.org/10.1017/jfm.2013.444 Published online by Cambridge University Press

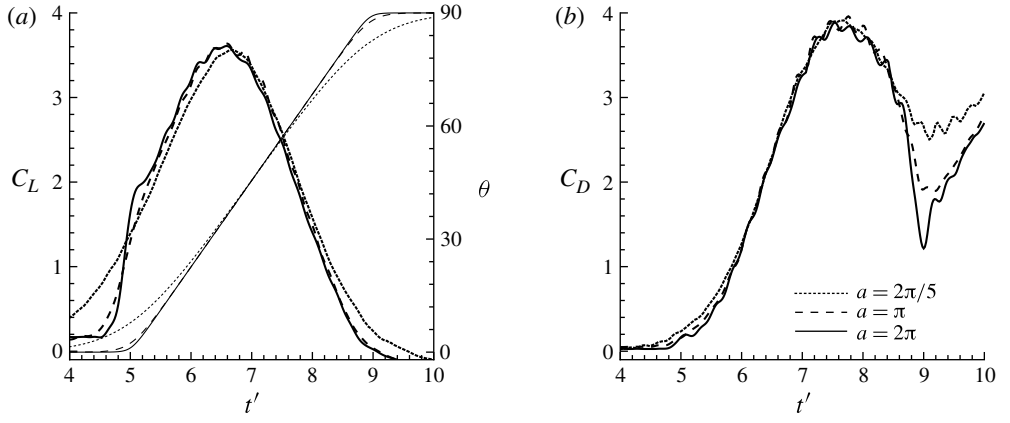


FIGURE 3. Lift (a) and drag (b) coefficients for different ramp corner smoothing for pitch rate of $K = 0.2$ with $x_p/c = 0$ leading edge pivot point. The curves in (a) show the ramp motion kinematics.

$$a = \frac{\pi^2 K}{2\theta_{max}\,(1-\sigma)} \tag{2.2}$$

$$t_2' = t_1' + \frac{\theta_{max}}{2K}. \tag{2.3}$$

3. Results

3.1. *Circulatory and non-circulatory forces*

We first consider the role of acceleration and non-circulatory force with different motion smoothing transients. Ol *et al.* (2010) compared a smoothed linear pitch ramp-hold-return manoeuvre, $\theta = 0°$–$45°$–$0°$, with a $45°\,(1 - \cos(\theta))$ function, such that the two would have identical peak pitch rates. The idea was to compare non-circulatory contributions, as the cosine function is always accelerating, while the smoothed linear function is accelerating only during the smoothing. A similar approach can be taken for the 0–90° pitch ramp, by varying the smoothing parameter σ from 0.5, 0.8 to 0.9, resulting in the $a = 2\pi/5$, π and 2π in (2.2). The motion ramp corner becomes progressively sharper, which affects the non-circulatory initial lift and final drag 'spikes' in figure 3.

At low angle of attack, this motion projects predominantly onto the lift direction, and as θ approaches 90°, onto the direction of drag. Thus, the acceleration in pitch at low θ produces a non-circulatory force that manifests itself as a positive increment in lift, while the deceleration in pitch at high θ results in a negative increment of drag. Indeed, a drop in drag is seen in figure 3(b) at high θ for higher accelerations. The relatively high overlap of all of the curves during the constant pitch rate in figure 3 is evidence of the success of linear superposition: circulatory and non-circulatory lift contributions are linearly additive and there is no effective 'flow memory' of a non-circulatory force, which was also concluded by Gendrich, Koochesfahani & Visbal (1995).

The 'ringing' in the force coefficients in the $a = 2\pi$ curve are from the model vibrating during the rapid acceleration at the ramp corners. More aggressive filtering

https://doi.org/10.1017/jfm.2013.444 Published online by Cambridge University Press

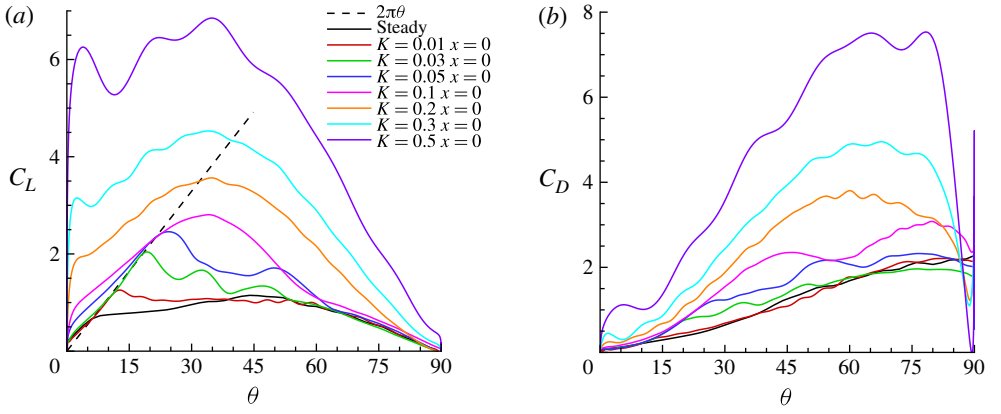


FIGURE 4. Lift (*a*) and drag (*b*) coefficients comparing pitch rate from static to $K = 0.5$ at constant pivot point $x_p/c = 0$.

would attenuate the effects of vibration, but also the non-circulatory spikes. The remainder of the parameter studies use $\sigma = 0.9$ for ramp corner smoothing.

3.2. *Pitch rate, pivot-point effects and kinematic scaling*

For the thin flat plate at the Reynolds number of the present experiments, the net aerodynamic force is normal to the plate. Lift and drag components are projections of the plate-normal force in the corresponding directions. At the lowest pitch rates considered here, $K < 0.01$–0.03, the effect of pitch rate is limited to stall delay, with the lift curve slope cleaving to 2π before stall in figure 4. At higher pitch rates, one can observe a departure of lift versus theta history even at low incidence angles: there is a strong rise in lift at low alpha, followed by a decrease in lift curve slope. Peak lift, and the incidence angle at which peak lift is attained, increase monotonically with increasing pitch rate through $K = 0.2$. At even higher pitch rates, peak lift coefficient continues to increase, but the incidence angle for peak lift saturates at $\approx 35°$. For $K = 0.3$, 0.5, and to a lesser extent 0.2, a bump in lift at $\theta \approx 5°$ is noticeable. This is the aforementioned non-circulatory lift increment.

The preceding discussion considered variation of pitch rate while the pitch pivot point was kept constant, at the plate's leading edge. Rate effects on aerodynamic force production are strongly mediated by choice of pivot point. Figure 5 considers the effect on lift and drag of five chordwise pivot point locations ($x_p/c = 0$, 0.25, 0.5, 0.75 and 1.0), while holding the pitch rate $K = 0.2$ constant. One observes monotonic decrease in C_L and C_D as the pivot point is taken further aft, while the incidence angle corresponding to peak-lift and -drag increases. Also notable is the behaviour of the non-circulatory lift spike at $\theta \approx 5°$. For midchord pivot point ($x_p/c = 0.5$), this spike is zero, while for pivot points further aft, it is actually negative. This result is also consistent with unsteady aerofoil theory (Leishman 2006). Similarly, there is a non-circulatory spike in drag coefficient corresponding to the pitch-stopping transient, with peak just before motion cessation. The symmetry in non-circulatory effects between lift (pitch-starting transient) and drag (pitch-stopping transient) is evidently explained by both spikes occurring in the plate-normal force. Indeed, the lift and drag peaks for each respective pitch-rate are comparable, suggesting that the dominant aerodynamic force is plate-normal.

https://doi.org/10.1017/jfm.2013.444 Published online by Cambridge University Press

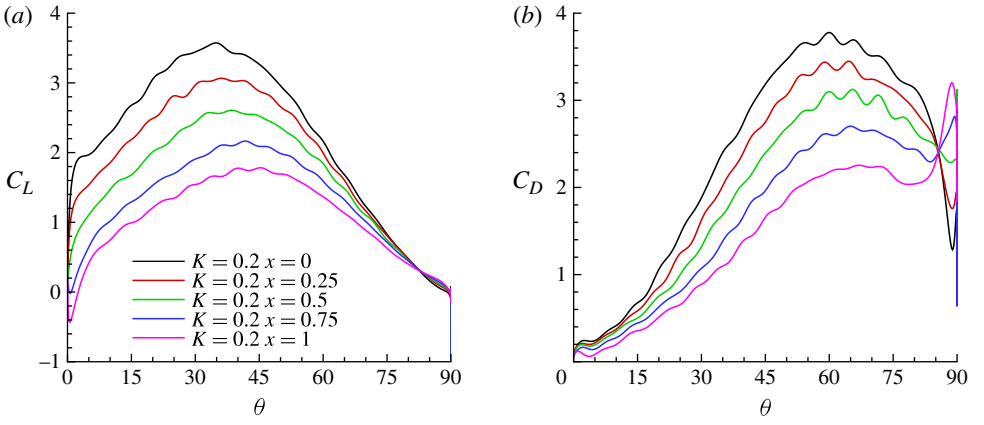


FIGURE 5. Lift (*a*) and drag (*b*) coefficients comparing pivot points $x_p/c = 0$, 0.25, 0.5, 0.75 and 1 at a constant pitch rate of $K = 0.2$.

Trends in lift and drag with pitch rate and pivot-point chordwise location offer tantalizing invitation to search for a unifying renormalization, whereupon all curves would ideally collapse onto one. Strickland & Graham (1987) proposed a scaling of lift and drag curves for a rapidly pitching wing according to (3.1) and (3.2) which are motivated by potential theory (Glauert 1947) ignoring leading-edge suction,

$$C_L(\theta) = 2A_L \sin\theta \cos\theta \tag{3.1}$$

$$C_D(\theta) = 2A_D \sin^2\theta \tag{3.2}$$

and using a linear fit of the constants A_L and A_D in (3.3) and (3.4) to peak lift and drag, respectively,

$$A_L = mK + n \tag{3.3}$$

$$A_D = oK + p. \tag{3.4}$$

Measurements by Yu & Bernal (2013) suggest that the reduction in lift upon taking the pitch pivot point further aft is due to increment of attached circulation opposing that producing positive lift. Unsteady aerofoil theory (Leishman 2006) predicts a contribution to lift due to pitch rate, linear in pitch rate and proportional to the distance from the pitch pivot point to the $x_p/c = 0.75$ point. If the pivot is itself at $x_p/c = 0.75$, any pitch rate contribution to lift should be zero. Figure 6 confirms this, in the sense that the various lift and drag curves across a K-range from 0.1 to 0.5 are quite similar, in contradistinction with the strong variation with respect to pitch rate in figure 4. Peak lift is around 2.1. This value is useful in generalizing the results of Strickland & Graham (1987) to account for pitch pivot point. If we linearize this pitch-rate contribution to

$$\alpha \approx \tan\alpha = \frac{w}{U_\infty} = \frac{\dot{\theta}\left(0.75 - x_p\right)c}{U_\infty} = 2K\left(0.75 - x_p\right). \tag{3.5}$$

The normal force coefficient from the pitch rate is

$$C_N = 2\pi\alpha = 4\pi K\left(0.75 - x_p\right). \tag{3.6}$$

https://doi.org/10.1017/jfm.2013.444 Published online by Cambridge University Press

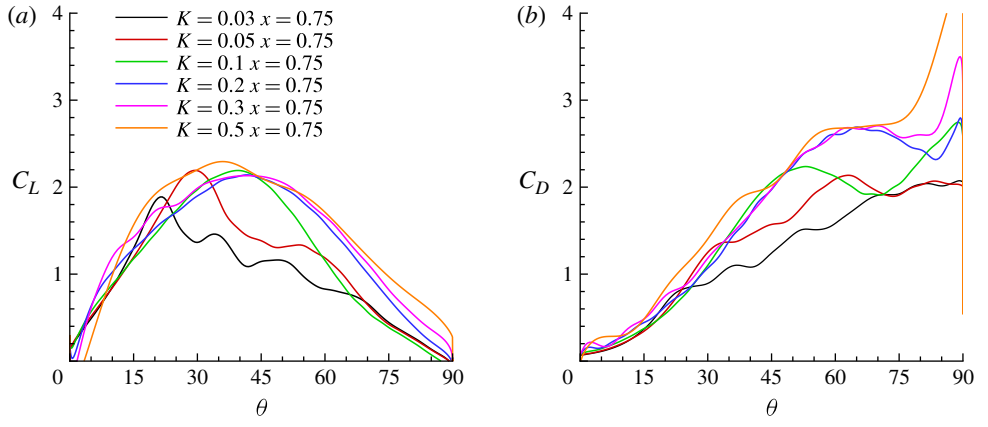


FIGURE 6. Lift (*a*) and drag (*b*) coefficients comparing pitch rates $K = 0.03$, 0.05, 0.1, 0.2 and 0.3 and 0.5 at a constant pivot point of $x_p/c = 0.75$.

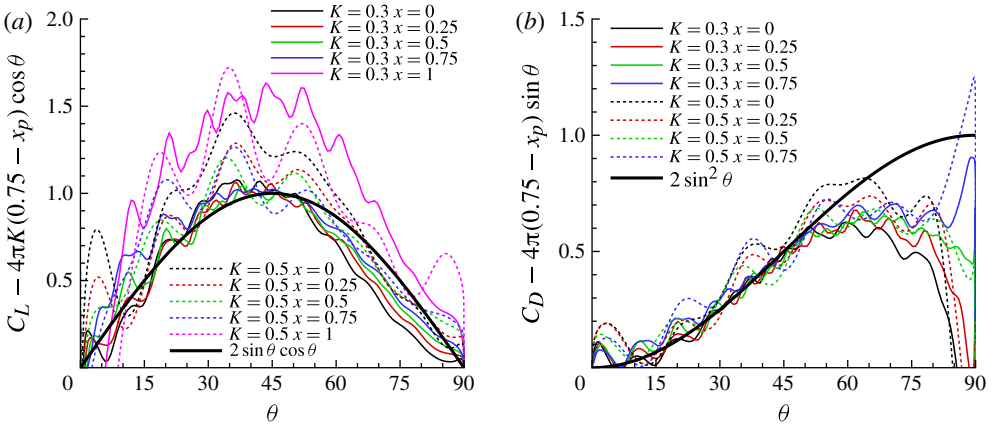


FIGURE 7. Collapse of lift (*a*) and drag (*b*) for pitch rates $0.3 < K < 0.5$ for new scaling function.

With this new contribution oriented in wind axis, the lift and drag coefficients now become

$$C_L = 2B_L \sin\theta\cos\theta + 4\pi K\left(0.75 - x_p\right)\cos\theta \tag{3.7}$$

$$C_D = 2B_D\sin^2\theta - 4\pi K\left(0.75 - x_p\right)\sin\theta. \tag{3.8}$$

If $B_L = 2.1$ in (3.7) from $C_{L,max} = 2.1$ when $x_p = 0.75$ and $B_D = 1$ in (3.8), the lift and drag curves collapse for all pivot points $x_p/c < 0.75$ in figure 7 up to $\theta = 45°$ as long as the pitch rate K is sufficiently large to not saturate the leading edge vortex (LEV) early in the motion. As shown in § 3.3, qualitative evidence of saturation and detachment of the LEV is accompanied by a decrease in net aerodynamic force. Therefore the early reduction of lift and drag forces shown in figures 4, 6 and 8 at low pitch rate is attributed to LEV saturation. For $\theta > 45°$ the collapse is better for higher pitch rates and more downstream pivot points.

Figures 7 and 8 consider the efficacy of collapse of lift and drag histories for various pitch rates and pivot points, when rescaled by (3.7) and (3.8). In figure 7,

https://doi.org/10.1017/jfm.2013.444 Published online by Cambridge University Press

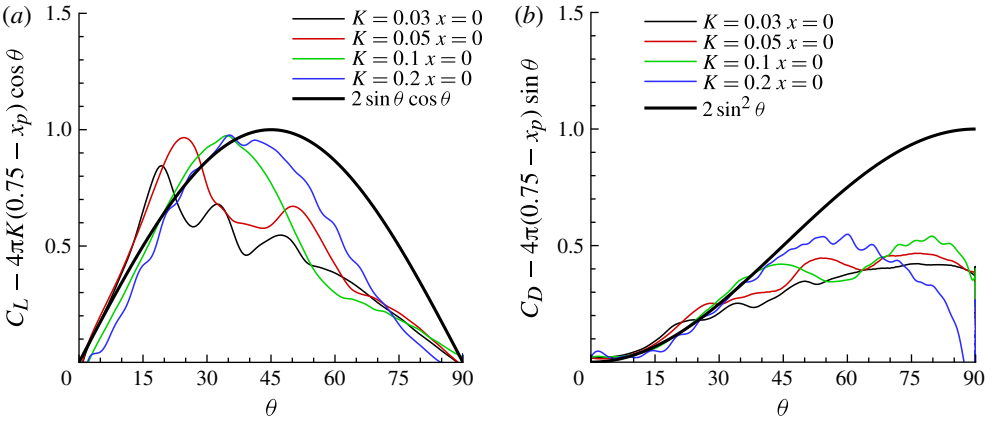


FIGURE 8. Lift (*a*) and drag (*b*) coefficients with pitch rate contribution subtracted for pitch rates $0.03 < K < 0.2$.

the $x_p/c = 1$ pivot-point cases are least amenable to the proposed scaling, while all cases with pivot point further forward (that is, $x_p/c \leqslant 0.75$) evince reasonable collapse to the $2\sin\theta\cos\theta$ curve. That is, the pitch-rate effect is successfully collapsed. In drag, collapse of the measured data to the $2\sin^2\theta$ curve (figure 7) is good up to $\theta \approx 60°$. The various runs are mutually similar through $\theta \approx 80°$, albeit diverging from the $2\sin^2\theta$ curve, before mutually diverging after $\theta > 80°$, where non-circulatory effects (which are not considered in the aforementioned scaling) take over. Figure 7 was for comparatively high pitch rates, $K = 0.3$ and 0.5. Figure 8 considers representative cases from $K = 0.03$ through $K = 0.2$. Assessment of success of the curve fit is of course subjective, but nominally $K = 0.1$ and 0.2 follow $2\sin\theta\cos\theta$ in lift and $2\sin^2\theta$ in drag through $\theta \approx 45°$, whereas the fit for $K = 0.03$ and 0.05 is considerably worse.

The better collapse of lift and drag for higher reduced pitch rates, with respect to the scaling in (3.7) and (3.8), suggests an alternative approach for the lower reduced pitch rates. One possibility is to shift the abscissa according to the pitch pivot point. That is, for a pivot about $x_p/c = 0.25$, one shifts the convective time against which lift or drag are plotted, by $t' = 0.25$, with respect to the $x_p/c = 0$ case; and so forth, for the other pivot points. This was done in figure 9 with the result of nearly coincident lift and drag (respectively) for the five pivot-point cases of $K = 0.03$, 0.05 and 0.10. As pivot point is taken further forward, lift increases; that is, the first peak C_L value, which now occurs for example for $K = 0.05$ at $t' \approx 9.5$, is higher. Any trend for peak drag magnitude dependence on pivot point cannot be observed at lower pitch rates. However, the respective rise in lift and drag is essentially coincident, with peaks occurring at essentially the same t' at $K = 0.03$ and 0.05, and somewhat less so for $K = 0.10$. This suggests two regimes of pitch rate: low rate, where shifting by convective time according to pivot point location is successful in bringing lift and drag curves into respective coincidence; and high rate, where scaling by pitch rate is effective. The intermediate or overlap region is $K \approx 0.1$–0.2, where neither (or both) approaches are completely successful. We also note that after the first peak in lift (or drag), there are subsequent peaks, evidently due to vortex shedding. These peaks also mutually collapse for $K = 0.03$, 0.05 and 0.10 in figure 9. This suggests that vortex-shedding events scale with convective time.

https://doi.org/10.1017/jfm.2013.444 Published online by Cambridge University Press

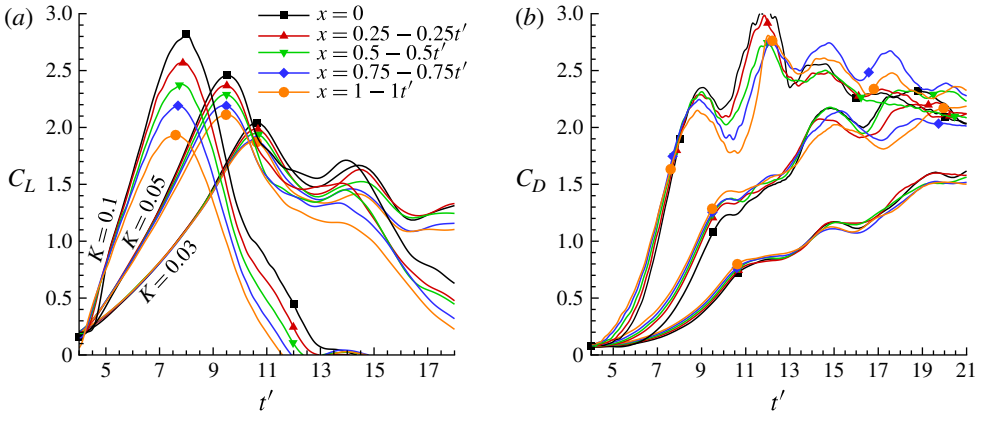


FIGURE 9. Collapse of lift (*a*) and drag (*b*) curves for pitch rates of $K = 0.03$, 0.05 and 0.1 for pivot points $x_p/c = 0$, 0.25, 0.5, 0.75 and 1. $K = 0.03$, 0.05 and 0.1 are shown grouped having corresponding increasing lift and drag.

3.3. *Vortex dynamics and convective scaling*

We now consider the relation between lift or drag history as function of incidence angle, pitch rate and pivot location, -vis the evolution of the flow field on the plates suction side. Figure 10 considers the $K = 0.2$, leading-edge pivot case with dye injection from leading and trailing edges at three spanwise locations: $y/(b/2) = 0.25$, 0.5 and 0.75. Snapshots are taken at incidence angles of 30, 45, 60 and 75°. Figure 10 compares flow field snapshots with history of normal force coefficient, as the net aerodynamic force is essentially plate-normal, and it is more intuitive to regard LEV effects on the plates suction side in a plate-referenced and not flow-referenced coordinate frame. We note that peak normal force coefficient occurs at ≈45° incidence, whereas peak lift for this case occurs at ≈34°. Qualitative rendition of vorticity in the near wake, and the leading edge shear layer and roll up show no discernable spanwise variation suggesting that two-dimensional assumptions in discussions of LEV and trailing edge vortex dynamics are appropriate. But the lack of spanwise variation of sectional flow field features does not imply lack of spanwise flow. Kurosaka *et al.* (1988) reported axial flow in vortices in a wall-bounded experiment and Koochesfahani (1989) likewise with end walls. Garmann & Visbal (2011) investigated a pitching aerofoil and concluded that the leading edge vortex is attached longer for increasing spanwise periodic computations from two dimensions to $s/c = 0.8$ which allows for spanwise relief of vorticity.

Correlation of leading edge vortex circulation growth, as a function of convective time (chords travelled by the free stream through a given attained plate incidence angle), with lift or drag history, suggests the idea of formation number (Gharib, Rambod & Shariff (1998), for vortex rings; Ringuette *et al.* (2007) and Baik *et al.* (2012) for pitching and plunging plates; also see review by Dabiri (2009)). This gives a non-dimensional convective time or plate incidence angle, for a given motion rate, by which the LEV circulation should saturate. Subsequently the LEV should pinch off from its feeding shear layer (Jones & Babinsky 2011). But the difficulty in elucidating a formation time is combining the pitch rate and pitch pivot-point location to arrive at a common reference length scale. It is well known that the LEV tightens as the pitch rate is increased (Visbal & Shang 1989; Graham & Yeow 1990; Ol *et al.* 2010), which

https://doi.org/10.1017/jfm.2013.444 Published online by Cambridge University Press

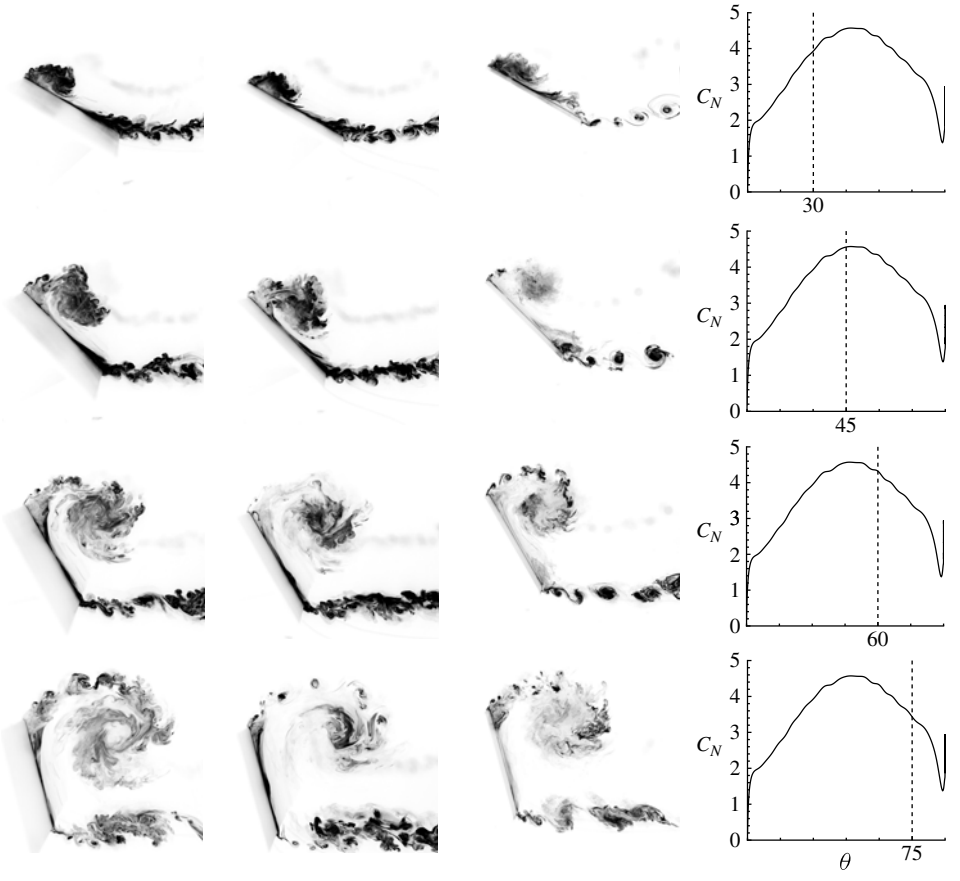


FIGURE 10. Dye flow visualization for 5/8 (left), 6/8 (mid) and 7/8-span (right) locations for $K = 0.20$, $x = 0$ pitch motion with corresponding normal force coefficient (far right). From top to bottom $\theta = 30°, 45°, 60°$ and $75°$.

ought to imply attainment of peak circulation earlier in the motion for higher reduced pitch rate K. In the following, we argue that LEV formation and growth is delayed as the pivot point is taken further downstream, while keeping pitch rate constant.

Although circumspection is merited in interpretation of dye concentration as surrogate for spanwise vorticity, qualitative correlations are still possible. Figure 10 is not sufficient to claim whether LEV circulation peaks simultaneously (or not) with the lift coefficient peak, but it is evident that a coherent LEV remains long after the normal-force peak. Figure 11 considers the $K = 0.2$ case for pivot at $x_p/c = 0$ and $x_p/c = 1$, taking a snapshot of the flow field at the incidence angle corresponding to peak lift in the first case and the second, one convective time later. From figure 5 one sees that peak lift for these two cases differs by approximately a factor of 2, and yet in figure 11, the two flow fields evince close qualitative similarity. This suggests that LEV history, and indeed also trailing edge wake history, scales with convective time; but that neither wake nor LEV similarity is sufficient to arrive at similarity of integrated aerodynamic force coefficient. That is, it is demonstrably not the case that a statement about flow field evolution carries reliable predictive power for aerodynamic force history at high motion rate. Though the present experiment does

https://doi.org/10.1017/jfm.2013.444 Published online by Cambridge University Press

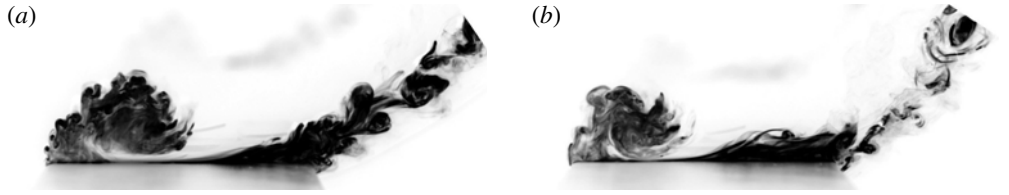


FIGURE 11. Flow visualization at peak lift for $K = 0.2$, $x_p/c = 0$ at $\theta = 34.2°$ (a) and $x_p/c = 1$ at $\Delta t' = 1$ later at $\theta = 57.1°$ (b). Images are rotated to plate coordinates.

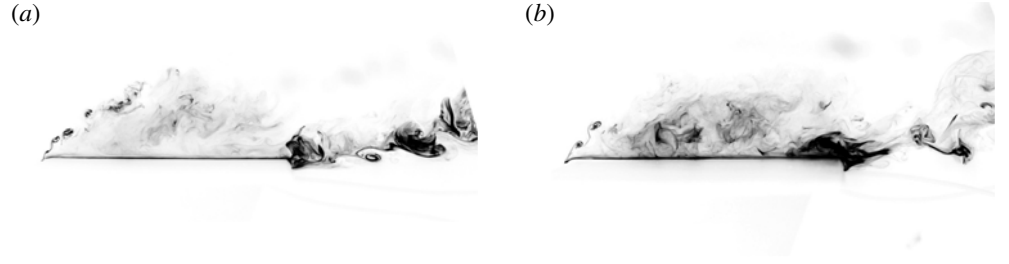


FIGURE 12. Dye flow visualization at peak lift for $K = 0.03$, $x_p/c = 0$ at $\theta = 19.3°$ (a) and $x_p = 1$ at $\Delta t' = 1$ later at $\theta = 22.4°$ (b). Images are rotated to plate coordinates.

not offer definitive prediction, one can ascribe this lack of aerodynamic force similarity to two likely causes: first, a vortex present near the pressure side of the wing, for the TE pivot case (Yu & Bernal 2013), but missing for the LE pivot case; and second, a difference in bound circulation between the LE pivot and TE pivot cases.

A contrary finding is apparent for the low-rate case, $K = 0.03$, in figure 12, which also compares $x_p/c = 0$ and $x_p/c = 1$ pivot points. Here the motion rate is evidently too slow to produce the qualitative rendition of a coherent LEV. The lack of LEV is consistent with the pre-stall lift curve in figure 4 not departing appreciably from the attached-flow thin aerofoil result of $C_L = 2\pi\alpha$. LEV presence or absence notwithstanding, as with the $K = 0.2$ case in figure 11, here again the $x_p/c = 0$ flow field qualitatively match the flow field snapshot for the $x_p/c = 1$ one convective time later, as expected from the time-base shifting in aligning lift and drag history in figure 9. One therefore finds that for a low pitch rate of $K = 0.03$, qualitative match in flow field evolution is congruent to match in lift evolution. As pitch rate increases, not only do pitch-rate effects become more important, but more interestingly, correspondence between flow field evolution and aerodynamic force evolution breaks down.

4. Conclusions

Aerodynamic forces and flow development for flat plates executing smoothed linear pitch ramps (0–90°) in a uniform stream were considered at different pitching rates ($0.01 < K < 0.5$) and pivot axis locations ($x_p/c = 0$, 0.25, 0.5, 0.75 and 1). The startup smoothing, being a region of non-zero acceleration, results in a non-circulatory lift transient, observable at $K = 0.2$ and above; a similar non-circulatory transient in drag is associable with the smoothing pitch-ramp conclusion. The latter is followed by gradual relaxation to steady state with vortex shedding. For reduced pitch rates

https://doi.org/10.1017/jfm.2013.444 Published online by Cambridge University Press

$0.01 < K < 0.03$, small departures from steady flow are observed, with peak lift significantly above steady stall value, but lift curve following the $C_L = 2\pi\alpha$ line of potential flow theory. For $K > 0.05$, pitch-rate and non-circulatory effects are observed, with strong dependency on reduced pitch rate and pivot axis location, qualitatively consistent with linear unsteady potential flow theory. Lift coefficient is proportional to reduced pitch rate and the distance between the pivot axis and the 3/4-chord location. The aforementioned non-circulatory spikes at pitch startup and cessation are proportional to the distance from the pivot axis to the mid chord and rotational acceleration. Changes in rotational acceleration (sharper motion transients) do not change aerodynamic forces during the constant pitch rate part of the motion, which supports linear superposition of non-circulatory and circulatory effects.

The correlation for lift and drag coefficients as functions of angle of attack developed by Strickland & Graham (1987) has been generalized to include pivot axis effects, evincing good agreement with experiment for $K > 0.1$. At lower reduced pitch rates, convective time is the main scaling parameter for flow evolution. A convective time shift equal to the pivot axis location normalized by the chord provides excellent temporal collapse of data, although maximum lift coefficient depends on pivot axis location possibly due to changes in vorticity distribution on the pressure side of the aerofoil (Yu & Bernal 2013).

At low reduced pitch rate a LEV does not form. At high reduced pitch rate, LEV formation is substantially two-dimensional, while the flow is highly three-dimensional at smaller scales. Across all reduced pitch rates, shifting of the time base according to the relative pivot axis location produces qualitative collapse of the leeward-side flow field, but at higher pitch rates (for example, $K = 0.2$), success of such flow field collapse does not ensure commensurate success in lift collapse. One might surmise that besides the usual LEV and near-wake vortical structures, a LEV on the plate's pressure side, formed early in the pitch-up motion, as well as differences in the bound circulation, are responsible for differences in magnitude of peak lift, and instance in time corresponding to the peak lift.

Acknowledgements

L.P.B. would like to acknowledge the support of the U.S. Air Force Office of Scientific Research, Multidisciplinary University Research Initiative (MURI), contract number FA9550-07-1-0547, Dr D. Smith program monitor.

References

Baik, Y., Bernal, L., Granlund, K. & Ol, M. 2012 Unsteady force generation and vortex dynamics of pitching and plunging aerofoils. *J. Fluid Mech.* **709**, 37–68.

Barlow, J. B., Rae, W. H. B., Rae, W. H. & Pope, A. 1999 *Low-Speed Wind-Tunnel Testing*, 3rd edn. Wiley.

Carruthers, A., Thomas, A. & Taylor, G. 2007 Automatic aeroelastic devices in the wings of a steppe eagle *aquila nipalensis*. *J. Expl Biol.* **210**, 4136–4149.

Chakravarthy, A., Grant, D. T. & Lind, R. 2012 Time-varying dynamics of a micro air vehicle with variable-sweep morphing. *J. Guid. Control Dyn.* **35** (3), 890–903.

Dabiri, J. 2009 Optimal vortex formation as a unifying principle in biological propulsion. *Annu. Rev. Fluid Mech.* **41**, 17–33.

Eldredge, J. D., Toomey, J. & Medina, A. 2010 On the roles of chord-wise flexibility in a flapping wing with hovering kinematics. *J. Fluid Mech.* **659**, 94–115.

https://doi.org/10.1017/jfm.2013.444 Published online by Cambridge University Press

GARMANN, D. & VISBAL, M. 2011 Numerical investigation of transitional flow over a rapidly pitching plate. *Phys. Fluids* **23** (9).

GENDRICH, C., KOOCHESFAHANI, M. & VISBAL, M. 1995 Effects of initial acceleration of the flow field development around rapidly pitching aerofoils. *J. Fluids Engng* **117**, 45–49.

GHARIB, M., RAMBOD, E. & SHARIFF, K. 1998 A universal time scale for vortex ring formation. *J. Fluid Mech.* **360**, 121–140.

GLAUERT, H. 1947 *The Elements of Aerofoil and Airscrew Theory*, 2nd edn. Cambridge University Press.

GRAHAM, G. M. & YEOW, K. F. 1990 Two-dimensional post stall maneuver of a NACA 0015 aerofoil at high pitching rates. *AIAA Paper* 1990-2810.

HARPER, P. W. & FLANIGAN, R. E. 1950 The effect of rate of change of angle of attack on the maximum lift of a small model. *NACA TN*-2061.

JONES, A. R. & BABINSKY, H. 2011 Reynolds number effects on leading edge vortex development on a waving wing. *Exp. Fluids* **51** (1), 197–210.

KOOCHESFAHANI, M. 1989 Vortical patterns in the wake of an oscillating aerofoil. *AIAA J.* **27** (9), 1200–1205.

KOOCHESFAHANI, M. & SMILJANOVSKI, V. 1993 Initial acceleration effects on flow evolution around aerofoils pitching to high angles of attack. *AIAA J.* **31** (8), 1529–1531.

KUROSAKA, M., CHRISTENSEN, W., TIRRES, L. & WOHLMAN, A. 1988 Crossflow transport induced by vortices. *AIAA J.* **26**, 1403–1405.

LEISHMAN, J. G. 2006 *Principles of Helicopter Aerodynamics*, 2nd edn. Cambridge University Press.

MCCROSKEY, W. J., CARR, L. W. & MCALISTER, K. W. 1976 Dynamic stall experiments on oscillating aerofoils. *AIAA J.* **14** (1), 57–63.

MCGOWAN, G. Z., GRANLUND, K. O., OL, M. V., GOPALARATHNAM, A. & EDWARDS, J. 2011 Investigations of lift-based pitch-plunge equivalence for aerofoils at low Reynolds numbers. *AIAA J.* **49** (7), 1511–1524.

OL, M. V., ALTMAN, A., ELDREDGE, J., GARMANN, D. & LIAN, Y. 2010 Summary of progress on pitching plates: canonical problems in low-Re unsteady aerodynamics. *AIAA Paper* 2010-1085.

OL, M. V., BERNAL, L. P., KANG, C.-K. & SHYY, W. 2009 Shallow and deep dynamic stall for flapping low Reynolds number aerofoils. *Exp. Fluids* **46** (5), 883–901.

REICH, G., EASTEP, F., ALTMAN, A. & ALBERTANI, R. 2011 Transient poststall aerodynamic modelling for extreme maneuvers in micro air vehicles. *J. Aircraft* **48** (2), 403–411.

RINGUETTE, M., MILANO, M. & GHARIB, M. 2007 Role of the tip vortex in the force generation of low-aspect-ratio normal flat plates. *J. Fluid Mech.* **581**, 453–468.

STRICKLAND, J. H. & GRAHAM, G. M. 1987 Force coefficients for a NACA 0015 aerofoil undergoing constant pitch rate motions. *AIAA J.* **54** (4), 622–624.

THEODORSEN, T. 1935 General theory of aerodynamic instability and the mechanism of flutter. *NACA R*-496.

VISBAL, M. & SHANG, J. K. 1989 Investigation of the flow structure around a rapidly pitching aerofoil. *AIAA J.* **27**, 1044–1051.

YU, H.-T. & BERNAL, L. P. 2013 Effect of pivot point on aerodynamic force and vortical structure of pitching flat plate wings. *AIAA Paper* 2013-0792.

https://doi.org/10.1017/jfm.2013.444 Published online by Cambridge University Press